Large-angle and high-efficiency tunable phase grating using fringe field switching liquid crystal

Daming Xu, Guanjun Tan, and Shin-Tson Wu[*]

CREOL, The College of Optics and Photonics, University of Central Florida, Orlando, Florida 32816, USA
[*]*swu@ucf.edu*

Abstract: We propose a switchable phase grating using fringe field switching (FFS) cells. The FFS phase grating possesses several attractive features: large diffraction angle, high diffraction efficiency, fast response time, and high contrast ratio. It can diffract >32% light to ± 2nd orders with a large diffraction angle of 12.1°. Meanwhile, its response time remains relatively fast even at −40°C. A simulation model is developed to explain the experimental results and good agreement is obtained. We also demonstrate a blazed phase grating to achieve tunable beam steering between 0th, 1st and 2nd orders.

©2015 Optical Society of America

OCIS codes: (160.3710) Liquid crystals; (050.1950) Diffraction gratings; (230.3720) Liquid-crystal devices.

References and links

1. M. Schadt, "Liquid crystal materials and liquid crystal displays," Annu. Rev. Mater. Sci. **27**(1), 305–379 (1997).
2. E. Lueder, *Liquid Crystal Displays: Addressing Schemes and Electro-Optical Effects* (Wiley, 2001).
3. Z. Luo, D. Xu, and S. T. Wu, "Emerging quantum-dots-enhanced LCDs," J. Disp. Technol. **10**(7), 526–539 (2014).
4. B. Maune, M. Loncar, J. Witzens, M. Hochberg, T. Baehr-Jones, D. Psaltis, A. Scherer, and Y. M. Qiu, "Liquid-crystal electric tuning of a photonic crystal laser," Appl. Phys. Lett. **85**(3), 360–362 (2004).
5. Y. H. Lin, H. S. Chen, H. C. Lin, Y. S. Tsou, H. K. Hsu, and W. Y. Li, "Polarizer-free and fast response microlens arrays using polymer-stabilized blue phase liquid crystals," Appl. Phys. Lett. **96**(11), 113505 (2010).
6. M. Xu, D. Xu, H. Ren, I. S. Yoo, and Q. H. Wang, "An adaptive liquid lens with radial interdigitated electrode," J. Opt. **16**(10), 105601 (2014).
7. F. Peng, D. Xu, H. Chen, and S. T. Wu, "Low voltage polymer network liquid crystal for infrared spatial light modulators," Opt. Express **23**(3), 2361–2368 (2015).
8. R. G. Lindquist, J. H. Kulick, G. P. Nordin, J. M. Jarem, S. T. Kowel, M. Friends, and T. M. Leslie, "High-resolution liquid-crystal phase grating formed by fringing fields from interdigitated electrodes," Opt. Lett. **19**(9), 670–672 (1994).
9. J. Chen, P. J. Bos, H. Vithana, and D. L. Johnson, "An electrooptically controlled liquid-crystal diffraction grating," Appl. Phys. Lett. **67**(18), 2588–2590 (1995).
10. D. P. Resler, D. S. Hobbs, R. C. Sharp, L. J. Friedman, and T. A. Dorschner, "High-efficiency liquid-crystal optical phased-array beam steering," Opt. Lett. **21**(9), 689–691 (1996).
11. P. F. McManamon, T. A. Dorschner, D. L. Corkum, L. Friedman, D. S. Hobbs, M. Holz, S. Liberman, H. Q. Nguyen, D. P. Resler, R. C. Sharp, and E. A. Watson, "Optical phased array technology," Proc. IEEE **84**(2), 268–298 (1996).
12. L. L. Gu, X. N. Chen, W. Jiang, B. Howley, and R. T. Chen, "Fringing-field minimization in liquid-crystal-based high-resolution switchable gratings," Appl. Phys. Lett. **87**(20), 201106 (2005).
13. I. Drevensek-Olenik, M. Copic, M. E. Sousa, and G. P. Crawford, "Optical retardation of in-plane switched polymer dispersed liquid crystals," J. Appl. Phys. **100**(3), 033515 (2006).
14. D. Subacius, P. J. Bos, and O. D. Lavrentovich, "Switchable diffractive cholesteric gratings," Appl. Phys. Lett. **71**(10), 1350–1352 (1997).
15. S. M. Morris, D. J. Gardiner, F. Castles, P. J. W. Hands, T. D. Wilkinson, and H. J. Coles, "Fast-switching phase gratings using in-plane addressed short-pitch polymer stabilized chiral nematic liquid crystals," Appl. Phys. Lett. **99**(25), 253502 (2011).
16. F. Fan, A. K. Srivastava, V. G. Chigrinov, and H. S. Kwok, "Switchable liquid crystal grating with sub millisecond response," Appl. Phys. Lett. **100**(11), 111105 (2012).
17. A. K. Srivastava, W. Hu, V. G. Chigrinov, A. D. Kiselev, and Y. Q. Lu, "Fast switchable grating based on orthogonal photo alignments of ferroelectric liquid crystals," Appl. Phys. Lett. **101**(3), 031112 (2012).

18. S. J. Ge, W. Ji, G. X. Cui, B. Y. Wei, W. Hu, and Y. Q. Lu, "Fast switchable optical vortex generator based on blue phase liquid crystal fork grating," Opt. Mater. Express **4**(12), 2535–2541 (2014).
19. J. Yan, Y. Li, and S. T. Wu, "High-efficiency and fast-response tunable phase grating using a blue phase liquid crystal," Opt. Lett. **36**(8), 1404–1406 (2011).
20. G. Zhu, J. N. Li, X. W. Lin, H. F. Wang, W. Hu, Z. G. Zheng, H. Q. Cui, D. Shen, and Y. Q. Lu, "Polarization-independent blue-phase liquid-crystal gratings driven by vertical electric field," J. Soc. Inf. Disp. **20**(6), 341–346 (2012).
21. J. Yan, Q. Li, and K. Hu, "Polarization independent blue phase liquid crystal gratings based on periodic polymer slices structure," J. Appl. Phys. **114**(15), 153104 (2013).
22. Y. T. Lin, H. C. Jau, and T. H. Lin, "Polarization-independent rapidly responding phase grating based on hybrid blue phase liquid crystal," J. Appl. Phys. **113**(6), 063103 (2013).
23. D. Xu, J. Yan, J. Yuan, F. Peng, Y. Chen, and S. T. Wu, "Electro-optic response of polymer-stabilized blue phase liquid crystals," Appl. Phys. Lett. **105**(1), 011119 (2014).
24. Y. Liu, S. Xu, D. Xu, J. Yan, Y. Gao, and S. T. Wu, "A hysteresis-free polymer-stabilised blue-phase liquid crystal," Liq. Cryst. **41**(9), 1339–1344 (2014).
25. D. Xu, J. Yuan, M. Schadt, and S. T. Wu, "Blue phase liquid crystals stabilized by linear photo-polymerization," Appl. Phys. Lett. **105**(8), 081114 (2014).
26. D. Xu, F. Peng, H. Chen, J. Yuan, S. T. Wu, M. C. Li, S. L. Lee, and W. C. Tsai, "Image sticking in liquid crystal displays with lateral electric fields," J. Appl. Phys. **116**(19), 193102 (2014).
27. H. Chen, F. Peng, Z. Luo, D. Xu, S. T. Wu, M. C. Li, S. L. Lee, and W. C. Tsai, "High performance liquid crystal displays with a low dielectric constant material," Opt. Mater. Express **4**(11), 2262–2273 (2014).
28. D. C. Flanders, D. C. Shaver, and H. I. Smith, "Alignment of liquid-crystals using submicrometer periodicity gratings," Appl. Phys. Lett. **32**(10), 597–598 (1978).
29. X. Y. Nie, R. B. Lu, H. Q. Xianyu, T. X. Wu, and S. T. Wu, "Anchoring energy and cell gap effects on liquid crystal response time," J. Appl. Phys. **101**(10), 103110 (2007).
30. S. T. Wu, "Nematic modulators with response time less than 100μs at room temperature," Appl. Phys. Lett. **57**(10), 986–988 (1990).
31. M. Schadt, "Low-frequency dielectric relaxations in nematics and dual-frequency addressing of field effects," Mol. Cryst. Liq. Cryst. (Phila. Pa.) **89**(1-4), 77–92 (1982).
32. H. Xianyu, S. T. Wu, and C. L. Lin, "Dual frequency liquid crystals: a review," Liq. Cryst. **36**(6-7), 717–726 (2009).
33. C. H. Wen and S. T. Wu, "Dielectric heating effects of dual-frequency liquid crystals," Appl. Phys. Lett. **86**(23), 231104 (2005).
34. D. K. Yang and S. T. Wu, *Fundamentals of Liquid Crystal Devices,* 2nd ed. (Wiley, 2014).
35. J. N. Li, X. K. Hu, B. Y. Wei, Z. J. Wu, S. J. Ge, W. Ji, W. Hu, and Y. Q. Lu, "Simulation and optimization of liquid crystal gratings with alternate twisted nematic and planar aligned regions," Appl. Opt. **53**(22), E14–E18 (2014).
36. J. W. Goodman, *Introduction to Fourier Optics* (McGraw-Hill, 1968).
37. S. T. Wu, "Birefringence dispersions of liquid crystals," Phys. Rev. A **33**(2), 1270–1274 (1986).
38. E. G. Loewen and E. Popov, *Diffraction Gratings and Applications* (Marcel Dekker, 1997).
39. E. Schulze and W. von Reden, "Diffractive liquid crystal spatial light modulators with fine-pitch phase gratings," Proc. SPIE **2408**, 113–120 (1995).
40. X. Wang, D. Wilson, R. Muller, P. Maker, and D. Psaltis, "Liquid-crystal blazed-grating beam deflector," Appl. Opt. **39**(35), 6545–6555 (2000).
41. J. W. Park, Y. J. Ahn, J. H. Jung, S. H. Lee, R. Lu, H. Y. Kim, and S. T. Wu, "Liquid crystal display using combined fringe and in-plane electric fields," Appl. Phys. Lett. **93**(8), 081103 (2008).

1. Introduction

In the past few decades, liquid crystal (LC) technology has undergone tremendous development incessantly. This ever-growing technology has now become indispensable not only in displays [1–3] but also in tunable photonic devices [4–7] due to its lightweight, low cost, and low power consumption. LC-based electrically tunable phase gratings [8–12] are among such components and have found widespread applications in optical interconnects, beam steering, three-dimensional displays, etc. In order to form a phase grating, the LCs need to have a periodically varying refractive index profile, which is usually produced by two types of electric field configuration. One uses a longitudinal electric field with patterned electrodes [9, 10, 12] whereas the other employs a transversal (TE) field generated by the interdigitated electrodes [8, 13]. However, with conventional nematic LCs, most of such gratings show slow response time (~10-100ms) and low diffraction efficiency (≤26%) [13, 14].

Recently, extensive efforts have been devoted to solve these problems [15–18]. In particular, tunable phase gratings using polymer-stabilized blue phase liquid crystal (PS-BPLC) showing submillisecond response time and high diffraction efficiency have been demonstrated [19–22]. But the major tradeoffs are twofold: high driving voltage (~150V) and noticeable hysteresis [22, 23]. Meanwhile, the PS-BPLC require special fabrication conditions, such as precise temperature control and UV polymerization [24, 25].

On the other hand, most the LC phase gratings using interdigitated (or in-plane switching, IPS) electrodes possess a small diffraction angle (~3°) [15, 19], which is too narrow for large-angle beam steering applications. The small diffraction angle originates from the large grating constant, which is determined by the dimension of IPS electrodes. The biggest challenge lies in the difficulties of fabricating small-dimension electrodes, thus there is limited space to further enhance the diffraction angle. Moreover, for the LC-based gratings investigated so far, their structural periodicity is fixed once fabrication is completed. Therefore, the diffraction angles cannot be tuned electrically.

In this paper, we propose a high-efficiency and large-angle phase grating using a fringe field switching (FFS) cell. The FFS phase grating can diffract >32% light to ± 2nd orders with a diffraction angle of 12.1°. And it possesses a high contrast ratio as well as fast response time (rise time 0.21ms and decay time 2.95ms at 23°C). Even at −40°C, the decay time is 40.4ms, which is still reasonably fast. To explain these experimental results, we construct a simulation model and obtain good agreement. Finally, we also demonstrate a blazed phase grating and achieve tunable beam steering between 0th, 1st and 2nd orders.
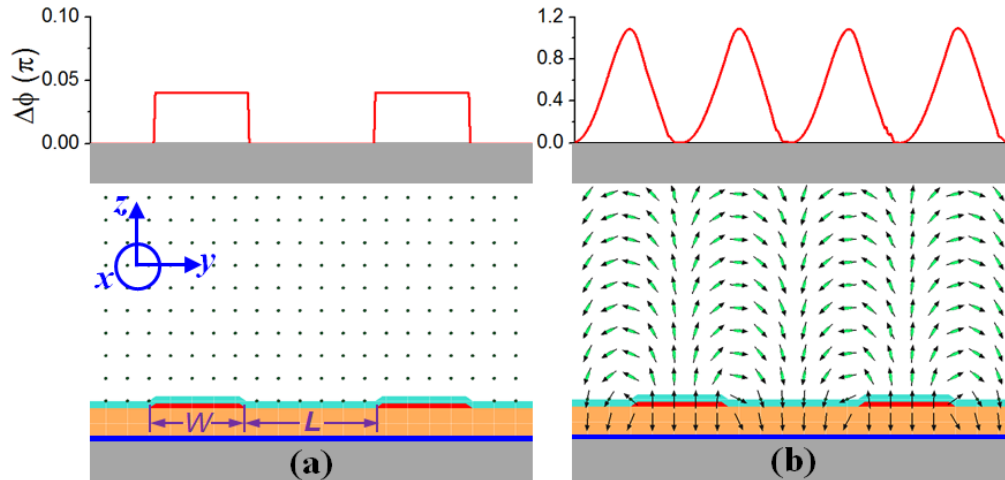
2. Physical principle

Fig. 1. Sketched phase LC director distributions (lower) and corresponding phase profiles for TM wave (upper) in an FFS cell under (a) 0V and (b) 35V applied voltage. The homogeneous alignment direction is 10° w.r.t. the pixel electrodes (x axis).

The LC director deformations of a FFS cell-based grating at voltage-off and voltage-on states are depicted in Figs. 1(a) and 1(b), respectively. The FFS cell is homogeneously aligned so that the phase change from the LC layer is uniform at different position along horizontal direction. Hence, the diffraction only comes from the index mismatch between the thin indium tin oxide (ITO) electrodes and the LC medium when no voltage is applied. Since the ITO layer is very thin (typically ~40 nm), the phase difference $\Delta\phi$ is very small, as shown by the phase profile in the upper plot of Fig. 1(a). As a result, its diffraction effect is very weak and can be neglected. The grating constant is $\Lambda_1 = (W + L)$, where W and L are the pixel electrode width and gap, respectively; as defined in Fig. 1(a). Hence, the diffraction angle θ_m can be calculated with following equation:

$$\sin\theta_m \cong m\lambda / n\Lambda_1,\qquad\qquad(1)$$

here m stands for the diffraction order, λ is the wavelength, and n is the average refractive index of LC layer.

As the applied voltage increases, the LC directors are reoriented gradually along the electric field, provided that the employed LC has a positive dielectric anisotropy ($\Delta\varepsilon>0$). Because of the non-uniform electric field in the FFS cell [26], the LC director distribution is not uniform as well, as Fig. 1(b) illustrates. The LC directors are vertically aligned by the electric fields on top of the pixel electrodes, whereas those are horizontally aligned at the gaps between the electrodes. Hence, the incident light would experience different phase changes at different positions along the horizontal direction and such a periodic phase distribution forms diffraction gratings. For qualitative illustration of the physical principle, we have calculated the phase difference of TM wave $\Delta\phi$ by integrating the phase change in each LC layer, as shown in the upper plot of Fig. 1(b). The phase difference becomes symmetric w.r.t. the center the electrode gap; as a result, the grating constant is reduced to $\Lambda_2 = \Lambda_1/2$. Accordingly, the diffraction angle is doubled compared to the voltage-off state, thus achieving a large-angle grating.

3. Experiment

To validate this concept, in experiment we prepared a FFS cell using UCF-L1, which is a low viscosity LC mixture developed by our group [27]. Its physical properties are listed as follows: $\Delta n = 0.121$, $\Delta\varepsilon = 2.89$, $\gamma_1 = 35$ mPa·s, $K_{11} = 10.2$ pN and $K_{22} = 5.5$ pN at $T = 23°C$, $\lambda = 633$ nm and $f = 1$ kHz. The FFS cell employed has pixel electrode width $W = 3$ μm, electrode gap $L = 4$ μm, cell gap $d = 3.65$ μm, and pretilt angle 2°. The cell is photo-aligned at 10° w.r.t. pixel electrode, and the dielectric constant of photo-alignment material is $\varepsilon = 3.9$. The passivation layer between the pixel and common electrodes is SiO_2 ($\varepsilon = 3.8$) with a thickness of 300 nm.

Figure 2(a) shows the experimental setup for optical measurement of the phase gratings. A He-Ne laser ($\lambda = 633$ nm) was used as probing beam. The transmission axis of the polarizer was set perpendicular to the pixel electrodes of the FFS cell in order to select the TM-polarized light [19]. An iris was placed behind the FFS cell to select the diffraction order and the intensity of the diffraction orders was detected by a photodiode in the far-field at a distance of ~30 cm.

At V = 0, the diffraction effect results from the periodicity of electrodes is quite weak and the laser power is mostly on the zeroth order, as Fig. 2(b) depicts. Although the higher orders can be observed, their intensity is negligible as compared to that of the zeroth order. Next, we drove the LC cell with a square-wave voltage at 1 kHz frequency. As the applied voltage increases, the periodic phase distribution appears and serves as a diffraction grating. Due to the aforementioned halved grating constant, the energy is transferred from the zeroth order to the 2nd order, as Fig. 2(c) illustrates. At 35V, the 2nd order has higher intensity than the 0th order, indicating that most of the light energy has been diffracted to the ± 2nd orders. The diffraction angle of the 2nd order is 12.1°. In contrast, there is no reduction in grating constant of the IPS cell when a voltage is applied. As a result, it is very challenging for IPS gratings to diffract light with such a large angle and comparable efficiency [15, 19]. Compared to IPS grating whose diffraction angle is ~3° at 1st order (highest-intensity order), our FFS phase grating exhibits a much larger diffraction angle. The diffraction angle can be further enhanced if we can reduce the electrode dimension of FFS cell [28]. Hence, the proposed FFS phase grating is promising for large-angle beam steering applications.
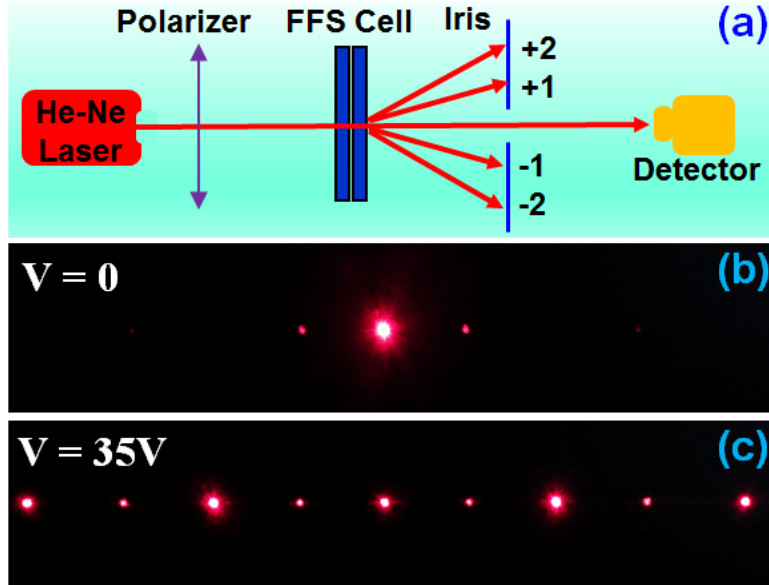
Fig. 2. (a) Experimental setup for measuring the diffraction efficiency. The iris is relocated to select the diffraction orders. (b) Recorded diffraction patterns at the voltage-off state. (c) Diffraction patterns at 35V. $\lambda = 633$nm and $T = 23°$.
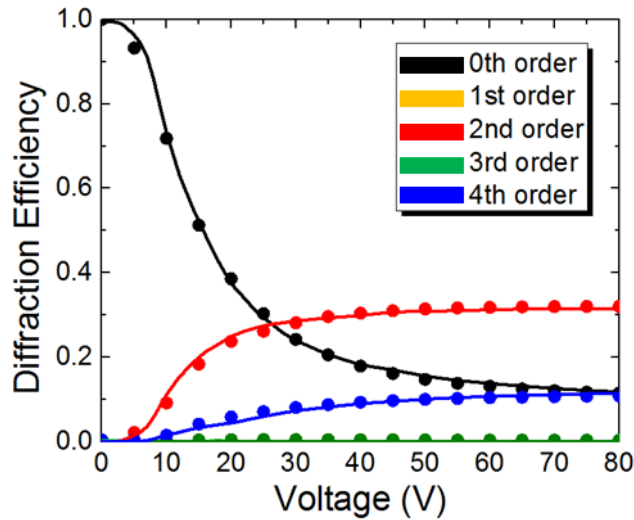

Fig. 3. Diffraction efficiency of the zeroth to fourth orders (Dots: measured data, solid curves: simulation results). Please note positive and negative orders have the same diffraction efficiency.

The dots in Fig. 3 show the measured diffraction efficiency of the zeroth to fourth orders. The diffraction efficiency η_m is defined as the ratio between the intensity of mth diffracted order and the total intensity at $V = 0$, described by Eq. (2):

$$\eta_m = I_m(V) / I_0. \qquad (2)$$

Figure 3 clearly shows that as voltage increases, some energy is transferred from 0th order to the even (e.g. 2nd, 4th, etc.) orders. However, the intensity of the 1st and 3rd orders are very weak, indicating the energy transferred to the odd orders is negligible. The diffraction efficiency is the same for the + 2 and −2 orders, both can achieve 32.1% at 70V with a

contrast ratio over 800:1. However, the diffraction efficiency gradually saturates in the high voltage region due to the strong anchoring effect of the LC cell [29]. Thus, if we are willing to sacrifice 2% in diffraction efficiency, then we can drive the FFS cell at 35V with 30% diffraction efficiency, which is still higher than that of traditional IPS phase gratings. The operation voltage can be further reduced if a larger $\Delta\varepsilon$ LC is employed.

Next, we measured the response time of the 2nd diffraction orders. Due to overdriving effect [30] from the high applied voltage (70V), the rise time is as fast as 0.21 ms at 23°C. Since the LCs are over-rotated from its rubbing direction at the on-state, as shown in Fig. 1(b), the elastic torque LC directors experience from the anchoring is very large during the relaxation process. Thus, the decay time is also very fast upon the removal of the applied voltage. The decay time of our FFS grating is 2.95 ms at 23°C. Both rise and decay times are much faster than those of nematic LC-based phase gratings (typically ~10-100 ms). More attractively, our phase grating using UCF-L1 still exhibits very fast response time even at low temperatures due to its ultra-low viscosity and low activation energy [27]. The measured decay time under different temperatures is plotted in Fig. 4. The decay time increases as the temperature decreases due to the increased viscosity. But even when the operation temperature drops to −40°C, the decay time is still as fast as 40.4 ms, which is much faster than the high-viscosity LCs, whose response time is usually around hundreds of milliseconds. Hence, our phase grating exhibits great potentials for low-temperature beam steering applications.
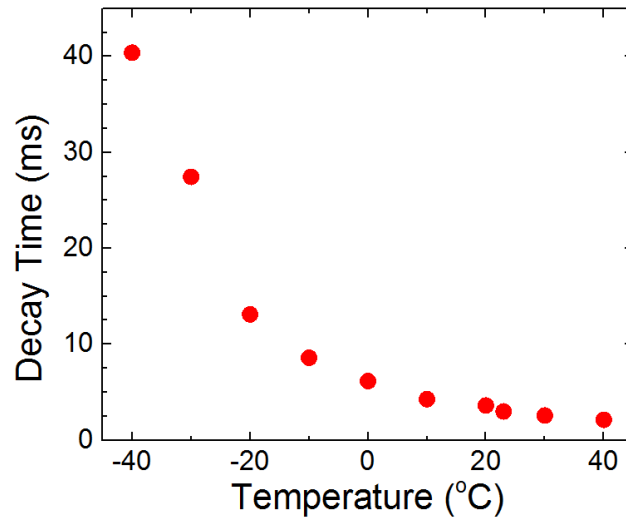

Fig. 4. Measured temperature-dependent decay time of FFS grating employing UCF-L1.

Another approach to obtain fast rise and decay time is to employ dual frequency liquid crystals (DFLCs) [31, 32]. In a DFLC device, a low-frequency voltage is used to turn-on while a high-frequency voltage is used to turn-off the LC phase modulator. As a result, both fast rise and decay times can be achieved. A major challenge of DFLC devices is noticeable dielectric heating effect [33] originated from the applied high frequency, which in turn causes the crossover frequency to drift. Therefore, for a DFLC device to work well, the operation temperature needs to be controlled precisely.

4. Simulation results

4.1 Numerical model

The physical principles of FFS gratings were qualitatively illustrated in Sec. 2, but without rigorous calculations. Therefore, we need to build a quantitative model to fit the experimental

data. It's worth mentioning here that for those LC gratings using uniform longitudinal electric field or blue phase liquid crystal, the polarization of incident light would not be changed. Hence, the phase profile can be calculated in a relatively easy way and the diffraction efficiency can be computed based on fast Fourier transforms. However, in our nematic FFS grating, the polarization of incident polarization light would be changed due to the rotation of LC molecules when a lateral field is applied, as shown in Fig. 1(b). Thus, we have to use the Jones matrix to track the polarization change in our model.

In our model, we first compute the LC director distribution using the finite element method [34], and this step can be done with commercial software TechWiz LCD (Sanayi, Korea). Then we utilized Jones matrix methods to calculate the output wavefront of the light. Since the grating constant $\Lambda \gg \lambda$, the light interference inside the grating is negligible and the periodic boundary condition can be applied here [35]. On the other hand, the LC medium is divided into many layers (~40 layers), thus the refractive index mismatch between adjacent LC layers is very small so that the reflection can be neglected. Based on these assumptions, the Jones matrix calculation method could be used here.

The direction of pixel electrode is defined as x-axis, and the polarization direction of the incident light, which is perpendicular to the pixel electrodes, is therefore set as y-axis. The light propagates along the z-axis. Hence, the Jones vector of the incident light is $\boldsymbol{J_0} = (0, 1)$. The LC bulk layer is divided into 40 layers and each layer can be considered as a wave plate and the Jones matrix of Nth layer can be represented as:

$$W_N = \begin{bmatrix} e^{jk_0 \cdot n_{eff} \cdot d} & 0 \\ 0 & e^{jk_0 \cdot n_o \cdot d} \end{bmatrix}, \tag{3}$$

where d is the thickness of the layer and n_{eff} is the effective index at the Nth layer:

$$n_{eff} = \frac{n_o \cdot n_e}{\sqrt{n_e^2 \cdot \sin^2 \theta + n_o^2 \cdot \cos^2 \theta}}. \tag{4}$$

Here, θ denotes the tilt angle of the LC directors. Therefore, the output electric field distribution along y-axis is the product of the Jones matrices of the whole LC layers and $\boldsymbol{J_0}$ [34]:

$$\begin{bmatrix} E_x(y) \\ E_y(y) \end{bmatrix}_{out} = R_N' W_N R_N ... R_2' W_2 R_1 R_1' W_1 R_1 J_1, \tag{5}$$

where R_N is the rotation matrix of the Nth layer and can represented by:

$$R_N = \begin{bmatrix} \cos\varphi & \sin\varphi \\ -\sin\varphi & \cos\varphi \end{bmatrix}. \tag{6}$$

Here, φ is defined as the azimuthal angle between the polarization of incident light and x-axis.

Since the diffracted light is detected by the photodiode at far field, here we can use the Fraunhofer diffraction equation [36] to model the diffraction pattern. Based on the calculated wavefront of output light, the diffraction efficiency is computed via fast Fourier transform:

$$E_x(k_y) = \int E_x(y) \cdot e^{-jk_y \cdot y} dy, \tag{7}$$
$$E_y(k_y) = \int E_y(y) \cdot e^{-jk_y \cdot y} dy.$$

Then the output intensity can be calculated from following equation:

$$I(k_y) = E_x(k_y)^2 + E_y(k_y)^2. \tag{8}$$

And the diffraction angle δ is determined by:

$$\sin \delta = k_y / k_0. \tag{9}$$

The simulated voltage-dependent diffraction efficiency curves using our model are also plotted in Fig. 3 as the solid curves. It is clearly shown that the simulation results overlap with the experimental data, indicating our model well describes the physical principles of FFS gratings. Hence, from here on we will use this model to further study the electro-optic properties of the FFS grating.

4.2 Phase retardation effect

The maximum diffraction efficiency (η_{max}) of the 2nd order depends on the phase retardation, or dΔn/λ of the FFS cell. The blue solid line in Fig. 5 depicts the calculated η_{max} at different dΔn/λ values for the FFS grating. As dΔn/λ increases from 0.4 to 1.0, η_{max} climbs to a peak of 33.4% at dΔn/λ ≈0.71 and then gradually decreases. To validate this phase retardation effect in experiment, we prepared three more FFS cells in addition to the one presented above using following materials: MLC-6686 [27], ZLI-1132 [37], and HAI-653265, all of which are commercially available materials. The first two are from Merck (Germany) and the third one is from HCCH (China). The parameters of FFS cells employed here are identical to the one discussed above except the cell gap. The material properties along with dΔn/λ values for these three cells are listed in Table 1. We measure the η_{max} of these three samples and plot them as the red squares in Fig. 5. We can see that the measured data show the same trend as discussed above. An attractive feature of FFS grating can be found in Fig. 5: in the 0.65 < dΔn/λ < 0.80 range η_{max} keeps larger than 98% of the peak value, which provides a reasonably large cell gap tolerance. Hence, we can choose dΔn/λ within this range during fabrication in order to achieve high diffraction efficiency of 2nd order.

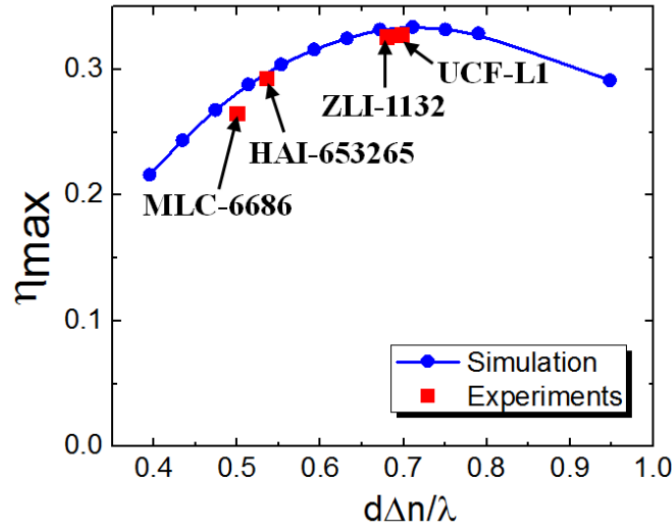Fig. 5. Maximum diffraction efficiency of the 2nd order at different dΔn/λ values for FFS gratings (λ = 633nm and T = 23°).

Table 1. LC material properties and corresponding dΔn/λ of three FFS cells (λ = 633nm, f = 1 kHz, T = 23°C).

LC	Δn	Δε	γ_1 (mPas)	K_{11} (pN)	K_{22} (pN)	K_{33} (pN)	dΔn/λ
MLC-6686	0.097	10.0	102	8.8	6.7	14.6	0.50
ZLI-1132	0.137	13.1	153	7.4	4.2	14.5	0.54
HAI-653265	0.096	2.3	44	13	7.8	14.2	0.68

5. Discussion

From the results presented above, the maximum 2nd order diffraction efficiency (~32%) of FFS grating is lower than that of a simple binary grating (~42%), in which perfectly rectangular phase profile is formed. Nevertheless, for most LC gratings, especially those employing nematic LCs, the diffraction efficiency is typically <26% [15]. Hence, our FFS grating exhibits a much higher diffraction efficiency than most nematic LC gratings with an additional advantage of large diffraction angle (~12°).

Nevertheless, for some applications such as imaging and 3D displays [38], high diffraction efficiency of the diffracted order is not the sole goal pursued. The diffraction ratio, which is usually defined as the ratio between diffraction efficiency of diffracted and 0th orders, is another important criteria for evaluating the phase grating performance. However, the experimental results in Fig. 3 only exhibit a diffraction ratio of ~3:1, which is relatively low and will generate cross-talk issues. In order to improve the diffraction ratio, we can optimize the $d\Delta n$ value by altering the cell gap or Δn, as shown in Figs. 6(a) and 6(b) are the simulation results of two FFS gratings using UCF-L1 with cell gap $d = 4$ and 5 μm, respectively. Compare to Fig. 3, we can see that the diffraction efficiency of 0th order is greatly reduced by increasing cell gap, leading to an enhanced diffraction ratio.
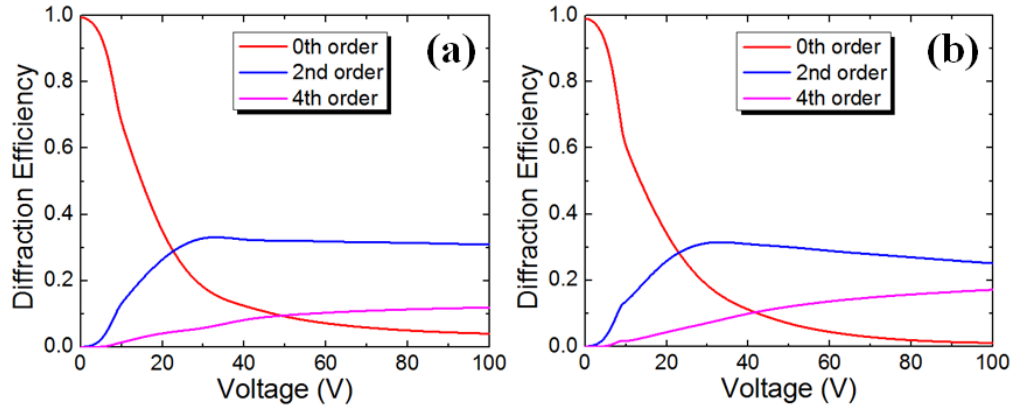

Fig. 6. Simulated diffraction efficiency of the 0th, 2nd, and 4th orders of the FFS gratings with different cell gaps: a) $d = 4$ μm; b) $d = 5$μm (LC: UCF-L1, $\Delta n = 0.121$).

This concept is also validated in experiments. Since the cell gap of our FFS cells are thinner than 4 μm, we choose to boost the Δn of LC in order to achieve a higher diffraction ratio. We prepared a FFS cell using LC with a higher $\Delta n = 0.146$. The measured diffraction efficiency of the 0th, 2nd, and 4th orders of this FFS cell are depicted in Fig. 7. In this case, the diffraction ratio is improved to ~30:1 at $V = 80V_{rms}$. By optimizing the $d\Delta n$ value, the diffraction efficiency of 0th order can be further reduced, and a high diffraction ratio is therefore obtained.
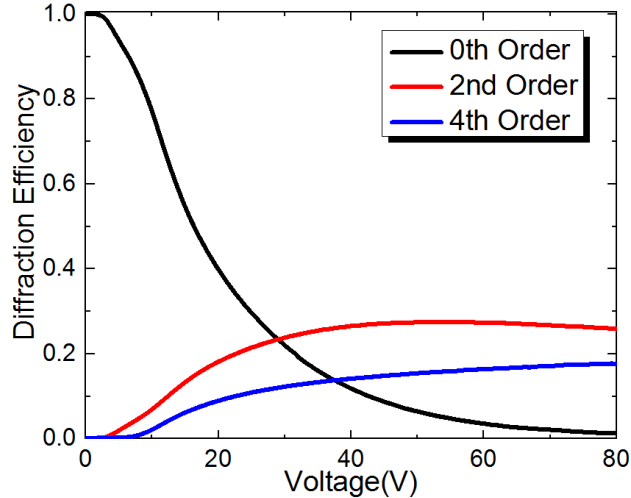
Fig. 7. Measured diffraction efficiency of the 0th, 2nd, and 4th orders in a FFS cell with $\Delta n = 0.146$.

6. Blazed phase grating

Blazed grating can be selected to achieve maximum diffraction efficiency in a given diffracted order [39, 40] and thus has widespread applications in fiber communications, microdisplays, optical scanners, etc [38]. However, for most of the LC-based gratings investigated so far, their structural periodicity is fixed once the fabrication is completed; thus the diffraction angles cannot be tuned electrically. Here, we propose a blazed phase grating that can be freely switched between 0th, 1st and 2nd orders using a fringe in-plane switching (FIS) cell [41]. The FIS mode was first proposed to reduce operation voltage and enhance transmittance for display applications. Here we employ this structure and modify its driving scheme to achieve a blazed phase grating. The device configuration is depicted in Fig. 8. The basic structure of the FIS cell remains the same as the FFS cell but the pixel electrodes are not necessarily in the same potential: adjacent pixel electrodes are applied with V_1 and V_2 voltages, respectively. To steer the light to $\pm$ 2nd orders, same voltage is applied to the adjacent pixels ($V_1 = V_2$) and the device operates in the same principle as the FFS cell. However, in order to steer the light to $\pm$ 1st orders, we keep V_1 and V_2 different so that not only a fringe field is formed between pixel and common electrodes but also an in-plane electric field is generated between pixel electrodes. Therefore, the grating constant is enlarged to $\Lambda = (W + L)$ again and more light are diffracted to $\pm$ 1st orders.
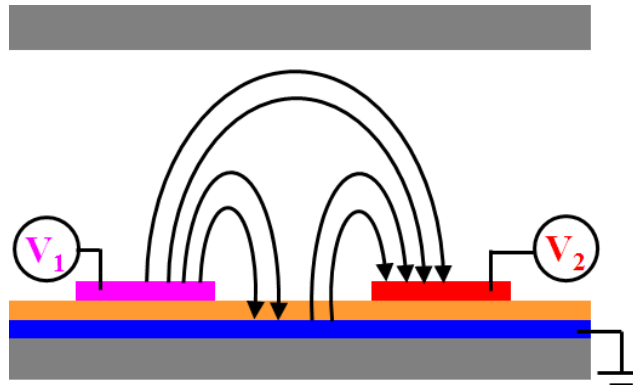

Fig. 8. Device configuration of the blazed grating using a FIS LC cell.

As discussed above, in order to achieving high diffraction ratio for reducing the cross-talk issue, here we optimized the dΔn values. Figure 9 depicts the simulated voltage-dependent diffraction efficiency of 0th, 1st and 2nd orders for this blazed grating. To reveal the energy transfer between different orders, V_1 is fixed at 50V and V_2 is scanned from −50V to 50V. From Fig. 9, when V_2 = −10V, the 1st order can achieve ~26% efficiency at a diffraction angle θ_1 = 5.9° whereas diffraction efficiency of the 2nd order is much lower, only 9.7%. This is because in-plane field exists between adjacent pixel electrodes and the grating constant is Λ = $(W + L)$, as illustrated by the phase profile in Fig. 10(a). As V_2 increases, more energy starts to transfer from 1st order back to 0th order. As V_2 exceeds 0V, energy starts to transfer to 2nd order since electric field between adjacent pixel electrodes becomes weaker and the symmetric LC director distribution w.r.t. the center of electrode gap starts to build up. When V_2 reaches the same potential as V_1, the electric field between adjacent pixel electrodes disappears and the device functions in the same way as the FFS cell, as shown in Fig. 10(b), thus directing the light onto the 2nd order with a diffraction efficiency of 29.4% at the diffraction angle θ_2 = 12.1°. Our blazed grating can switch between 0th, 1st and 2nd orders flexibly, thus potential use of more applicable gratings by optimizing cell gap, Δn, and driving voltages are foreseeable.
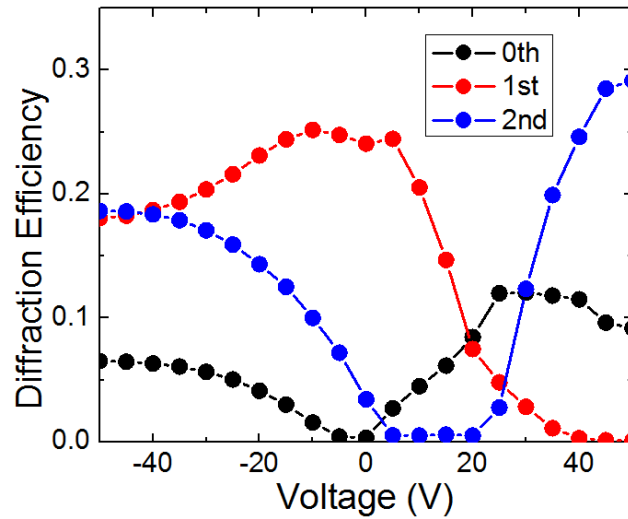

Fig. 9. Simulated diffraction efficiency of 0th, 1st and 2nd orders when V_2 is scanned from −50V to 50V (V_1 is fixed at 50V). Cell gap = 5.0μm. λ = 633 nm.
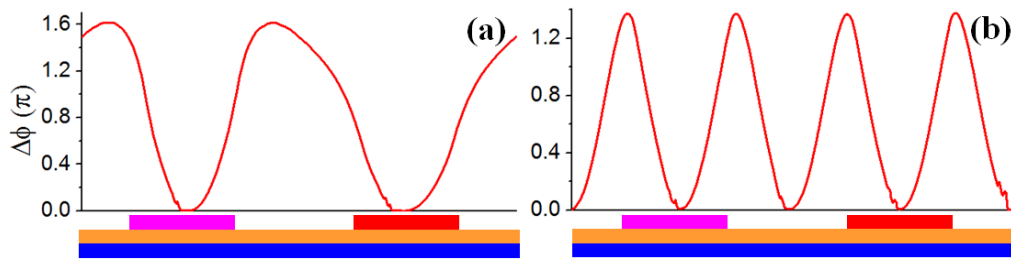

Fig. 10. Simulated phase profile of FIS grating under (a) V_2 = −10V and (b) V_2 = 50V. V_1 is fixed at 50V (λ = 633 nm).

7. Conclusion

We have proposed switchable phase grating using a FFS cell. The FFS phase grating possesses several attractive features: large diffraction angle, high diffraction efficiency, fast

response time, and high contrast ratio. It can diffract >32% light to ± 2nd orders with a diffraction angle of 12.1°. Meanwhile, it is able to achieve a rise and decay time of 0.21ms and 2.95ms, respectively. Even when the phase grating operates at −40°C, it still exhibits a reasonably fast decay time of 40.4ms. A simulation model is developed to explain the experimental results and good agreement is obtained between the model and experiment. Moreover, a blazed phase grating is proposed to achieve tunable beam steering between 0th, 1st and 2nd orders.

Acknowledgments